remote sensing

MDPI

Article

Assessment of Glacier Transformation in China over the Past 40 Years Using a China-Specific Glacier Classification System

Tianya Li [1], Yuzhe Wang [1,*], Baojuan Huai [1], Hongmin An [1,2], Lei Wang [1] and Weijun Sun [1]

[1] College of Geography and Environment, Shandong Normal University, Jinan 250014, China; litianya@stu.sdnu.edu.cn (T.L.); 616070@sdnu.edu.cn (B.H.); anhm@sdnu.edu.cn (H.A.); leiwang@sdnu.edu.cn (L.W.); sunweijun@sdnu.edu.cn (W.S.)
[2] School of Management, Shandong University, Jinan 250100, China
* Correspondence: wangyuzhe@sdnu.edu.cn

Abstract

Glacier classification offers a structured framework for assessing glacier characteristics and understanding their responses to climate change. In this study, we apply the Shi–Xie glacier classification system, proposed by Chinese glaciologists Shi and Xie, to evaluate the transformation of extremely continental, subcontinental, and maritime glaciers across China over the past four decades. Our results show a widespread rise in equilibrium line altitudes (ELAs), alongside complex changes in climatic and glaciological parameters. Notably, despite ongoing warming trends, nearly half of the glaciers experienced cooling at the ELA, and over two-thirds showed a decline in summer mean temperatures. This apparent contradiction is explained by elevation-induced cooling; as ELAs rise to higher altitudes, the corresponding summer air temperatures decline due to the lapse rate effect. Near-surface ice temperatures (20 m depth) were strongly consistent with changes in annual air temperature. Precipitation trends were spatially heterogeneous, yet around 70% of glaciers experienced stable or slightly increasing annual precipitation. In contrast, maritime glaciers, particularly those in the southeastern glacierized regions, exhibited marked decreases. Glacier surface velocities generally declined, with 90% of glaciers flowing at speeds below 50 m a^{-1}. Threshold-based analysis reveals that glaciers in transitional zones frequently exhibit multi-indicator deviations. Extremely continental glaciers near classification boundaries showed a shift toward warmer, wetter subcontinental conditions, while maritime glaciers tended toward drier, colder subcontinental characteristics. These findings offer new insights into the differentiated responses and ongoing transformation of glacier types in China under climate change.

Keywords: Chinese glacier change; glacier classification; glacier transform; continental glacier; maritime glacier

Academic Editor: Ulrich Kamp

Received: 26 April 2025
Revised: 30 June 2025
Accepted: 1 July 2025
Published: 3 July 2025

Citation: Li, T.; Wang, Y.; Huai, B.; An, H.; Wang, L.; Sun, W. Assessment of Glacier Transformation in China over the Past 40 Years Using a China-Specific Glacier Classification System. *Remote Sens.* **2025**, *17*, 2289. https://doi.org/10.3390/rs17132289

1. Introduction

China hosts the largest number and total volume of glaciers at mid and low latitudes globally [1]. These glaciers are concentrated on the Tibetan Plateau (TP) and its surrounding mountain ranges, including the Himalayas, Kunlun Mountains, Karakoram, Tien Shan, Hengduan Mountains, Qilian Mountains, and Altai Mountains. They provide crucial meltwater to downstream regions, which is essential for socio-economic developments in arid and semi-arid areas [2,3]. Spanning a vast geographic area, Chinese glaciers exhibit considerable spatial variability in hypsography, morphology, and ice flow dynamics. They

are influenced by distinct atmospheric circulations, governed by the Indian monsoon and westerlies, with limited contributions from the East Asian monsoon [4]. Over the past two decades, climate change has driven significant glacier retreat [5], mass loss [6,7], surface velocity slowdown [8], rising snowline altitude [9–11], and an increase in extreme geohazards, including large-volume detachments [12–14] and glacial lake outburst floods [15–17]. These changes exhibit considerable spatial and temporal variability [5,18], largely driven by the glacier diversity and regional climate differences across China. To better understand these variations, a classification system is crucial for examining how different glacier types respond to climate change. However, few studies have applied a classification-based approach to Chinese glaciers, limiting insights into climate-induced impacts on distinct glacier types.

Glaciers have been categorized based on geographical distribution (e.g., Himalayan or Arctic type), source of nourishment (e.g., central firn cap or dendritic glacier system), thermal regime (e.g., cold or polythermal type), climatic zone (e.g., tropical or continental type), and morphology (e.g., valley glacier or ice cap) [19]. These classification systems are widely used in glaciology for diverse studies. Given the extensive distribution of Chinese glaciers across various climatic zones and mountain ranges, Shi and Xie developed a classification system, hereafter referred to as the Shi–Xie classification, based on climatic and geophysical criteria [20]. This system categorizes glaciers into three types, i.e., extremely continental, subcontinental and maritime. The Shi–Xie classification, subsequently refined with more detailed quantifications by later researchers [21–23], has been widely applied in textbooks [23], tourism development [24], and the guidance of typical glacier monitoring programs [25]. It is extensively used in glaciological studies across both China and High-Mountain Asia (HMA) [26–28]. However, existing studies have largely focused on glacier type characteristics and the application of classification schemes, while lacking long-term, regional-scale assessments of glacier type transformations. Therefore, assessing glacier changes by glacier type, as defined by the Shi–Xie classification, is crucial. Such an assessment would enhance our understanding of two key aspects: whether glacier changes cause deviations from classification thresholds and whether glaciers transition from one type into another.

This study assesses changes in different glacier types across China over the past four decades, based on the criteria defined by the Shi–Xie classification. We focus particularly on glaciers located near the boundaries between types, as these are most sensitive to rapid climate change. Using climate reanalysis data, remote sensing data, and numerical models, we calculate the classification criteria and investigate their spatio-temporal changes for individual glaciers. We also examine potential transformations between glacier types over the study period. This paper is structured as follows: First, we introduce the study area and selected glaciers. Next, we describe the multi-source datasets and methods used for climate data downscaling, equilibrium line altitude (ELA) modeling, and near-surface ice temperature modeling. Then, we analyze changes in classification criteria during 1981–2000 and 2001–2020. Finally, we discuss the mechanisms driving the observed glacier changes and present our conclusions.

2. Study Glaciers

According to the second Chinese Glacier Inventory (CGI2), the total glacier area is approximately 43,087 km^2 [1]. Extremely continental, subcontinental, and maritime glaciers make up 32%, 46%, and 22% of this area, respectively. To investigate glacier type changes over the past four decades, we selected representative glaciers for detailed analysis based on the following criteria. First, all three glacier types should be included to ensure comprehensive representation. Second, glaciers from diverse mountain ranges should be chosen

to capture climatic and glaciological variability. Third, glaciers should be valley types with areas ranging from 10 to 40 km^2, excluding surging glaciers. Lastly, glaciers should be situated near the boundaries of the three glacier types to capture the potential temporal variability of glacier characteristics. Ultimately, 80 glaciers were selected (Figure 1, Table S1), including 31 extremely continental glaciers, 33 subcontinental glaciers, and 16 maritime glaciers. Among these, six glaciers with relatively long-term, comprehensive observations were used to calibrate and validate our calculated glacier criteria (Figure 1, Table S2).

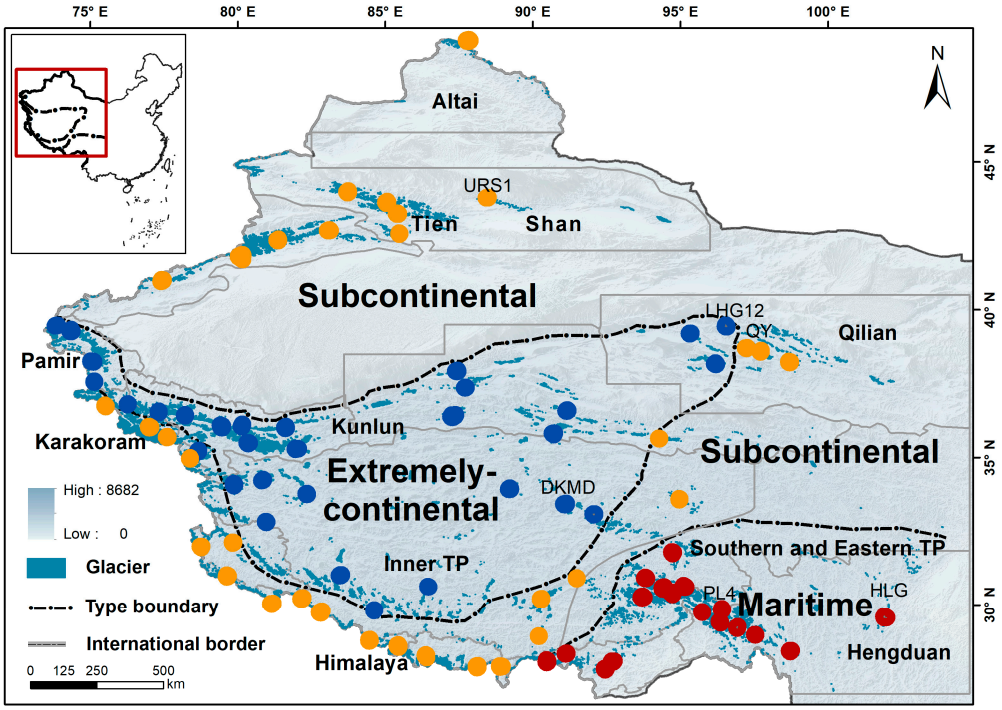

Figure 1. Distribution of three different types of glaciers in China. Glacier outlines are indicated by light blue polygons. Gray outlines indicate the HMA subregions located in China. The dashed lines indicate the boundaries of the glacier type regions based on the Shi–Xie classification. The blue, yellow, and red dots indicate the selected extremely continental, subcontinental, and maritime glaciers, respectively. The background image is the USGS GTOPO30 DEM. The inset shows the location of glacierized regions in China.

3. Data and Methods

3.1. Shi–Xie Classification Method

The Shi–Xie classification system divides glaciers into extremely continental, subcontinental, and maritime types using five key glaciological and climatological criteria [20,29]. These criteria include the following: (1) the annual mean temperature at the ELA (T_a), (2) the annual total precipitation at the ELA (P_a), (3) the summer mean temperature (June–August) at the ELA (T_s), (4) the annual mean ice temperature at a depth of 20 m at the ELA (T_{20}), and (5) the maximum velocity along the glacier centerline (v). Each glacier is assigned a type according to thresholds, as listed in Table 1, which collectively reflect its climatic and dynamic conditions.

Table 1. The Shi–Xie glacier classification scheme.

Type	T_a (°C)	T_s (°C)	P_a (mm)	T_{20} (°C)	v (m a^{-1})
Extremely continental	<−10	<−1	200–500	<−10	30–50
Subcontinental	−12~−6	0~3	500–1000	−10~−1	50–100
Maritime	>−6	1~5	1000–3000	−1~0	>100

3.2. Glacier Outlines

We selected representative Chinese glaciers based on the criteria described in Section 2, using the CGI2 v1.0 as our primary dataset. The Randolph Glacier Inventory Version 6.0 (RGI 6.0), although integrating glacier outlines from both the GAMDAM v1.0 and CGI2 v1.0 inventories within the HMA region depending on regional data availability and quality, was not used for initial glacier selection because it lacks information on glacier national affiliation and omits some glaciers located within China's borders. To extract the main centerlines of the selected glaciers, we utilized the publicly available global glacier centerline dataset generated by the Open Global Glacier Model (OGGM) v1.4 [30], which is based on RGI 6.0. Fortunately, the Chinese glaciers we selected from CGI2 are also included in RGI 6.0, allowing for cross-referencing between the two datasets. By matching each glacier in CGI2 with its corresponding RGI ID, we extracted the main centerline for each glacier. These centerlines were subsequently used to extract glacier surface elevations and surface velocities along the flowlines. In addition, boundaries of different glacier types defined by the Shi–Xie classification were manually digitized based on the map provided in [29].

3.3. DEMs

DEMs are used to derive the elevation of grid cells in the reanalysis dataset and to determine the ELAs. Elevation data for the reanalysis grid are obtained from SRTM30_PLUS v11, a global topography and bathymetry dataset with a spatial resolution of 30 arc seconds (approximately 1 km) [31]. SRTM30_PLUS was developed using multiple data sources, with land topography derived from SRTM and ICESat data. The ELA is computed by the OGGM through surface mass balance (SMB) modeling [30]. For this purpose, we configured OGGM to use the SRTM V4.1 DEM with a spatial resolution of 90 m to derive the ELA.

3.4. ELAs

ELA is the altitude on a glacier where ablation equals accumulation for the year. According to the classification criteria outlined in Table 1, ELA plays a crucial role in deriving the basic glaciological and climatological characteristics in the Shi–Xie classification. We calculate the ELAs over the period 1981–2019 by modeling the annual mass balance using the OGGM v1.6 [30]. OGGM utilizes the temperature-index method to model the SMB with climate forcing inputs from GSWP3-W5E5 (see Section 3.5) [32]. To derive the ELA in a hydrological year, we first model the monthly mass balance along the glacier elevation bands. The SMB $B_i(z)$ in each elevation band z and month i is calculated as follows:

$$B_i(z) = P_i^{solid}(z) - f_{snow/ice} max(T_i(z) - T_{melt}, 0), \quad (1)$$

where P_i^{solid} is the monthly solid precipitation, $f_{snow/ice}$ are the degree-day factors for ice or snow, T_i is the monthly temperature, and T_{melt} is the threshold temperature above which ice/snow melt is assumed to occur (here set to -1 °C). The surface air temperatures at different elevation bands were extrapolated using a constant monthly lapse rate -6.5 K km^{-1}.

In OGGM, three key parameters control the SMB model, the degree-day factor, precipitation correction factor, and temperature bias. OGGM calibrates these parameters glacier by glacier against the geodetic mass balance dataset from [7], covering the period 2000–2019. The calibrated parameters are then applied to compute monthly SMB profiles over the entire study period. The annual ELA is subsequently determined as the altitude at which the net annual SMB equals zero.

To assess long-term glacier changes while minimizing the impact of interannual variability, we define two reference periods, i.e., 1982–2000 and 2001–2019, based on the

multi-year ELA time series (1981–2019). These periods are consistently used throughout this study to compare changes in the Shi–Xie classification criteria.

3.5. Meteorological Data at ELA

Meteorological data are essential for deriving glaciological and climatological criteria in the Shi–Xie classification. In this study, we extract 2 m air temperature and precipitation from the ERA5-Land climate reanalysis dataset. Many studies have evaluated the performance of ERA5-Land in the HMA mountain regions, finding that it effectively captures the spatio-temporal patterns and extremes of temperature and precipitation.

For SMB modeling and ELA calculation, OGGM uses the bias-adjusted ERA5 reanalysis data, specifically the GSWP3-W5E5 dataset, as its standard climate input. This dataset combines W5E5 data with homogenized GSWP3 data, providing global coverage at a 0.5° spatial resolution [32,33]. The high resolution and robust bias correction of GSWP3-W5E5, particularly for extreme values, make it well-suited for accurately modeling glacier SMB.

To calculate the 2 m air temperature (T_{ELA}) and precipitation (P_{ELA}) at the ELA of each glacier, we use the ERA5-Land monthly averaged data spanning the period from 1980 to 2020. The closest ERA5-Land grid cell to each glacier's centroid is referred to as the reference grid. We first extract the time series of 2 m temperature at the reference grid cell (T_{ref}). The elevation of the reference grid (z_{ref}) is then determined by masking the SRTM30_PLUS DEM. Assuming a constant lapse rate (γ_T) of -6.5 K km^{-1}, T_{ELA} is computed through linear interpolation as

$$T_{ELA} = T_{ref} + \gamma_T \left(z_{ELA} - z_{ref} \right). \tag{2}$$

P_{ELA} is calculated following the interpolation method proposed by Huss and Hock [34]. To estimate the precipitation gradient, we first identify the level-7 HydroBASINS sub-basin in which each glacier is located. HydroBASINS provides globally consistent, hierarchically nested drainage basin boundaries [35]. Within each glacier's sub-basin, we extract all reanalysis grid cells and perform a linear regression between their precipitation values and elevations to derive the local absolute precipitation gradient (γ_{abs}, unit: mm per 100 m). The relative precipitation gradient (γ_{rel}; unit: % per 100 m) is then calculated using the following equation:

$$\gamma_{rel} = \frac{\gamma_{abs}}{\overline{P}_{basin}}, \tag{3}$$

where $\overline{P}_{basin}$ is the average precipitation over the glacier's sub-basin [36]. P_{ELA} is calculated as follows:

$$P_{ELA} = \alpha_P \cdot P_{ref} \left(1 + \left(z_{ELA} - z_{ref} \right) \cdot \gamma_{rel} \right), \tag{4}$$

where P_{ref} is the precipitation at the reference grid cell and α_P is a correction factor to account for potential biases in the precipitation data.

This elevation-adjusted downscaling ensures that both T_{ELA} and P_{ELA} reflect glacier local conditions more accurately than using coarse grid values alone. Moreover, 20-year climatological means are used to suppress short-term variability and enhance stability in classification.

3.6. Near-Surface Ice Temperature

The near-surface ice temperature (0–20 m depth) is influenced by the atmosphere and associated heat–water transport process. To estimate the long-term impacts of climate change on near-surface thermal state at the ELA, we only consider the heat conduction process and assume that the ice temperature at 20 m depth (T_{20}) does not fluctuate with

seasonal atmosphere change. A one-dimensional heat conduction model is used to simulate the vertical temperature profile:

$$\frac{\partial T}{\partial t} = \frac{k}{\rho c_p} \frac{\partial^2 T}{\partial z^2}, \tag{5}$$

where T is the ice temperature, t is the time, k is the thermal conductivity of ice, ρ is the ice density, and c_p is the specific heat capacity of ice. Equation (5) is numerically solved using the finite difference method. We first assume the initial temperature profile of the ice column at the ELA is isothermal and equals to the annual mean surface air temperature from the previous year. The basal boundary condition is set to zero heat flux. We then use the daily ERA5-Land air temperature to force this model over the hydrological year. We take the modeled temperature profile to represent the near-surface thermal state at the ELA.

3.7. Glacier Surface Velocities

Glacier surface velocities are the sum of contributions from both ice deformation and basal sliding. Monitoring the long-term changes in surface glacier velocity can enhance our understanding of glacier dynamics and their evolution. Due to logistical challenges and remoteness, glacier velocity measurements in China are restricted to a few glaciers and are not continuous both in space and in time [37]. Benefiting from achievements in remote sensing techniques, a few global-scale glacier velocity products are now publicly available [38–40]. In this study, we use the ITS_LIVE (Inter-Mission Time Series of Land Ice Velocity and Elevation) product developed by NASA to estimate glacier surface velocities. ITS_LIVE offers high-resolution velocity data (240 m) spanning from 1985 to 2018, derived from Landsat 4, 5, 7, and 8 satellite imagery using the auto-RIFT processing chain. Although the ITS_LIVE velocity dataset does not fully cover 1982–2019, it spans the two ELA reference periods sufficiently. We use the 1985–2000 and 2001–2018 means to represent the first (1982–2000) and second (2001–2019) periods, assuming they reflect long-term glacier dynamics. From this dataset, we extract the maximum flow speed for each glacier along its centerline, which was generated by OGGM using the method proposed by [41].

4. Results

4.1. Calibration and Validation

Precipitation in mountainous regions is spatially heterogeneous due to rugged topography and is less well-constrained because of sparse rain gauge data. To address this, we calibrated the parameters γ_{rel} and α_P in our precipitation interpolation method using observed precipitation data from six glaciers (see Table 2). The results show that the adjustment factor α_P ranges from 0.60 to 1.15, with higher values observed for maritime glaciers, such as the PL4 and HLG glaciers. The precipitation gradient γ_{rel} varies from −3.4%/100 m to 4.5%/100 m, indicating significant spatial variability. Notably, γ_{rel} is negative for maritime glaciers and positive for continental glaciers. For the subsequent analysis, we used the average values of γ_{rel} and α_P derived from these six glaciers for precipitation interpolation. A sensitivity analysis of the impact of γ_{rel} on the derived glacier criteria in the Shi–Xie classification is provided in Section 5.

To validate the modeled ELAs by OGGM, we compared them with observed ELAs from six representative Chinese glaciers covering different glacier types and regions (Table S3). As shown in Figure 2, the modeled ELAs generally agree well with the observations. Some deviations may stem from uncertainties in the reanalysis climate data, downscaling methods, and degree-day factors. Despite these discrepancies, the modeled ELAs offer a reliable foundation for deriving the criteria defined in the Shi–Xie classification.

Table 2. Calibration of precipitation interpolation parameters based on measurements from six glaciers.

Glacier	α_P	γ_{rel}	Altitude	Time Period
LHG12	0.76	4.5%/100 m	4500 m	2010–2015
DKMD	0.82	1.4%/100 m	4600 m	2008–2010
QY	0.61	2.4%/100 m	4870 m	2008–2012
URS1	0.60	4.1%/100 m	3700 m	2002–2004
PL4	1.15	−1.9%/100 m	4600 m	2008–2018
HLG	0.79	−3.4%/100 m	3500 m	1980 and 2000

LHG12 = Laohugou Glacier No. 12, DKMD = Dongkemadi Glacier, QY = Qiyi Glacier, URS1 = Urumqi River Source Glacier No. 1, PL4 = Parlung Glacier No. 4, HLG = Hailuogou Glacier.

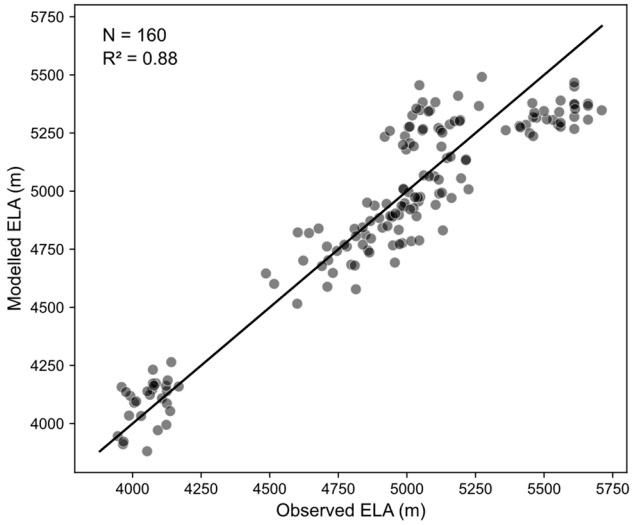

Figure 2. The linear regression of modeled ELAs and observed ELAs.

We further validated the calculated glacier criteria at the ELA, including T_a, P_a, T_s, and T_{20}, with available observations. As shown in Figure 3, the modeled values generally show strong agreement with observations, with R^2 values ranging from 0.61 to 0.92. The highest correlations were observed for T_s and T_{20}, indicating good model performance for summer and near-surface ice temperatures. While some discrepancies remain, particularly for T_a, the overall results demonstrate the reliability of the calculated criteria within the Shi–Xie classification framework.

4.2. Spatio-Temporal Distribution of ELAs and Glacier Criteria

We assessed the spatial distributions of the classification criteria for the periods 1982–2000 and 2001–2019 and compared their temporal changes between these two periods. Although the ELA itself is not one of the five classification criteria in the Shi–Xie classification, it is essential for deriving the other criteria. Therefore, we present the spatio-temporal patterns of the ELA alongside the five core criteria.

4.2.1. Distribution over the Period 1982–2000

1. ELA

The spatial distributions of ELAs and the five classification criteria for the study glaciers during the period 1982–2000 are shown in Figure 4. The ELA distribution exhibited both latitudinal and longitudinal zonality (Figure 4a). Overall, ELAs decrease from the Himalayas to the Altai Mountains, ranging from 6138 m to 3247 m. In contrast, ELAs increased from the eastern periphery of the TP toward its interior and the western Himalayas, with values ranging from 4800 m to 6100 m. The lowest ELAs were found in the Tien

Shan and Altai Mountains, averaging around 4000 m. Other regions with relatively low ELAs include the Pamir, Karakoram, Kunlun Mountains, Qilian Mountains, Hengduan Mountains, and eastern TP. In contrast, the highest ELAs were concentrated in the inner TP and the Himalayas, with values generally around 6000 m.

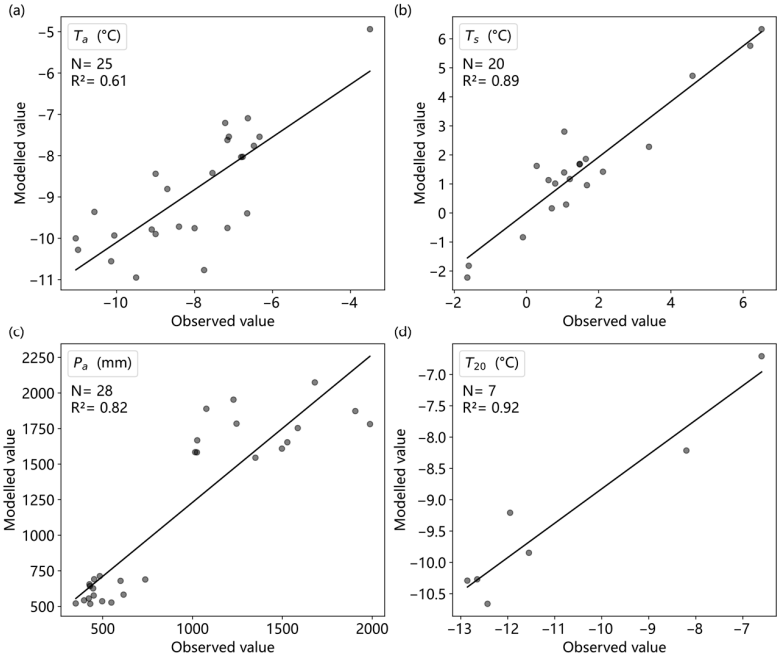

Figure 3. Validation of glacier criteria against observations. (**a**) T_a, (**b**) T_s, (**c**) P_a, and (**d**) T_{20}.

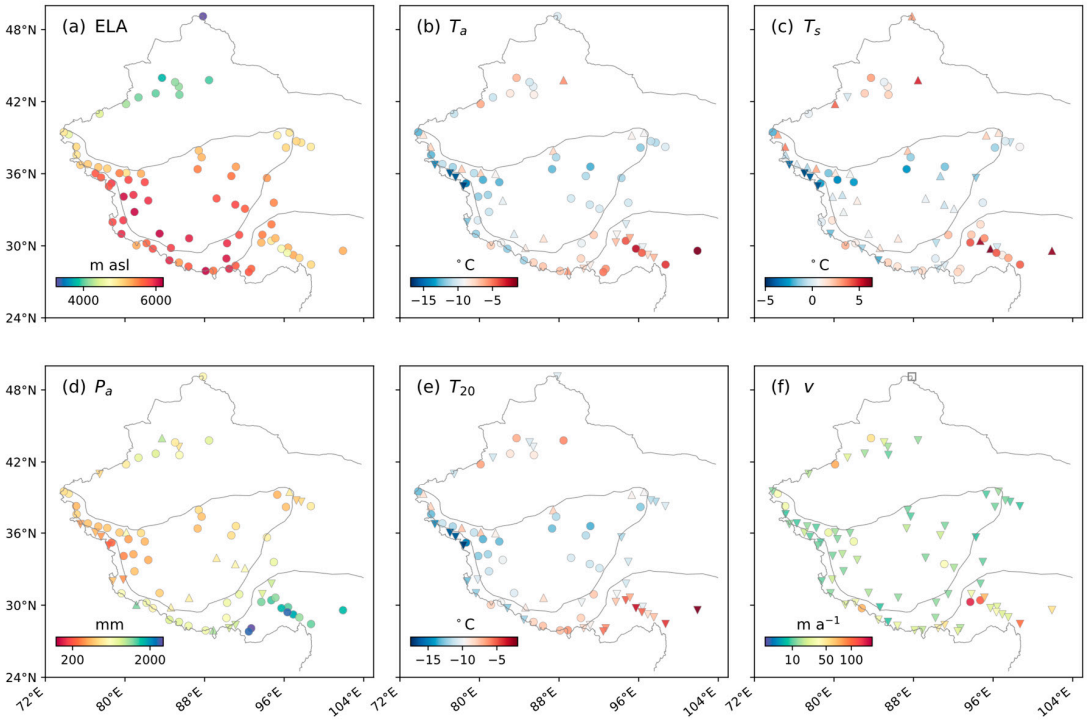

Figure 4. Distribution of ELAs and classification criteria over the period 1982–2000. (**a**) ELA, (**b**) T_a, (**c**) T_s, (**d**) P_a, (**e**) T_{20}, (**f**) v. Circles indicate that there are no changes in individual glacier criteria relative to the threshold of their corresponding glacier type. Upper triangles indicate that the criterion values for individual glaciers exceed the thresholds of their respective glacier types, while lower triangles indicate that the criterion values fall below these thresholds. The square in panel (**f**) indicates glaciers with no velocity data.

Among the three glacier types, extremely continental glaciers had the highest mean ELA at 5459 m, followed by maritime glaciers at 5302 m and subcontinental glaciers at 5125 m. All three types exhibited substantial spatial variability due to their wide geographical distributions. Subcontinental glaciers, which span the largest geographical area from the Himalayas to the Altai Mountains, showed the greatest variability, with ELAs ranging from 3247 m to 6138 m and a standard deviation of 811 m. Maritime glaciers, primarily located in the eastern Himalayas, southern and eastern TP, and Hengduan Mountains, exhibited the lowest variability, with a standard deviation of 372 m. For extremely continental glaciers, ELAs generally increased toward the interior of the TP, peaking at 6137 m.

2. Annual mean temperature at ELA (T_a)

The distribution of T_a (Figure 4b) showed that the highest T_a values were found in the southeastern part of the study region, including the Hengduan Mountains, eastern Himalayas, and southern and eastern TP, where glaciers were predominantly maritime. In contrast, the lowest T_a values were observed in the Pamir, Karakoram, and Kunlun Mountains. The eastern and central Himalayas, as well as the Tien Shan, also exhibited relatively high T_a values. Glaciers in the inner TP displayed moderate T_a values compared to other regions.

When compared to the thresholds of T_a for individual glacier types, we found that more than one-third of the glaciers deviated from their respective thresholds, with 14 glaciers exceeding and 14 glaciers falling below their thresholds. The glaciers with T_a values below their corresponding thresholds were primarily maritime (nine glaciers) and subcontinental types (five glaciers), concentrated in the Karakoram and the southeastern part of the study region, including the Nyainqentanglha, Hengduan Mountains, and eastern Himalayas. In contrast, the glaciers with T_a values exceeding their thresholds were mostly extremely continental (12 glaciers, more than 85%) and 2 subcontinental glaciers. These extremely continental glaciers were located in the inner TP, Kunlun Mountains, Pamir, and Qilian Mountains, while the two subcontinental glaciers exceeding the threshold were located in the eastern Tien Shan and eastern Himalayas.

3. Summer mean temperature at ELA (T_s)

The spatial pattern of T_s (Figure 4c) closely resembled that of the annual mean temperature T_a (Figure 4b). Over 60% of glaciers had a summer mean temperature above 0 °C ($T_s > 0$ °C), spanning various mountain ranges and encompassing different glacier types. Almost all maritime glaciers (13 out of 16) exhibited $T_s > 0$ °C. Similarly, nearly all subcontinental glaciers in the Tien Shan and Altai Mountains had $T_s > 0$ °C. Extremely continental glaciers with $T_s > 0$ °C were predominantly located at the boundary between extremely continental and subcontinental glacier types. In contrast, extremely continental glaciers with $T_s < 0$ °C were mainly concentrated in the Kunlun Mountains, inner TP, and Pamir. Subcontinental glaciers with $T_s < 0$ °C were primarily located in the Karakoram and Himalayas.

Compared to the T_s thresholds in the Shi–Xie classification, we found that more than one-third of the glaciers had T_s values surpassing their respective thresholds (28 glaciers), while 19% had T_s values falling below the thresholds (15 glaciers). The remaining 46% of glaciers (37 glaciers) stayed within their corresponding threshold limits. Among the glaciers whose T_s values went above the threshold values, the majority were extremely continental glaciers (79%), predominantly located in the inner TP and Kunlun Mountains. For glaciers with T_s values below the specified thresholds, 80% were subcontinental glaciers, mainly found in the Himalayas and Karakoram, with only three maritime glaciers and no extremely continental glaciers.

4. Annual precipitation at ELA (P_a)

Figure 4d shows the spatial distribution of P_a, which exhibited a distinctly polarized pattern. P_a values generally exceeded 1100 mm in the Hengduan Mountains, with extremes surpassing 2000 mm, while in the western Kunlun Mountains, they were less than 400 mm. High P_a values (>900 mm) were concentrated in the southeastern part of China's glacierized regions, including the Hengduan Mountains, eastern Himalayas, and Nyainqentanglha, where glaciers were predominantly maritime. In contrast, regions with low precipitation (<400 mm) were found in the Kunlun Mountains, inner TP, Karakoram, western Himalayas, and Qilian Mountains, where glaciers were primarily extremely continental.

During the period 1982–2000, P_a values for 70% of the glaciers (56 out of 80) remained within their respective thresholds. Approximately 13% of glaciers exhibited increasing precipitation trends, with P_a values surpassing their corresponding thresholds. These glaciers were mainly located in the inner TP, with a few scattered in the Himalayas, Kunlun Mountains, Qilian Mountains, and Tien Shan. Meanwhile, 17% of glaciers showed a decrease in P_a, with values falling below their threshold limits. These were primarily subcontinental glaciers, located in the Karakoram, western Himalayas, Qilian Mountains, and Tien Shan.

5. Annual mean 20 m ice temperature (T_{20})

The spatial pattern of T_{20} over the period 1981–2000 closely mirrors that of T_a (Figure 4e). High-T_{20} areas were concentrated in the southeastern part of the study region, coinciding with regions of high T_a. In contrast, low T_{20} values were found mainly in the Karakoram, Kunlun Mountains, and Pamir Mountains, which are among the colder glacierized regions in China.

When comparing T_{20} values to the thresholds for each glacier type, we observed that the changes in T_{20} were not consistent with those in T_a. Approximately 42.5% of glaciers remained within their respective T_{20} thresholds, primarily located in the inner TP, Kunlun Mountains, Tien Shan, and Himalayas, and mostly belonging to the extremely continental type. Around 45% of glaciers experienced a decrease in ice temperature, falling below their respective T_{20} thresholds. These glaciers were primarily located outside the extremely continental glacier zone. All maritime glaciers and 60% of subcontinental glaciers had T_{20} values below their thresholds. Only 12.5% of glaciers (10 out of 80) surpassed their T_{20} thresholds, indicating warmer near-surface ice temperatures; all of these were all extremely continental glaciers located in the Kunlun Mountains, Pamir, inner TP, and Qilian Mountains.

6. Maximum glacier surface velocity (v)

Figure 4f illustrates the spatial distribution of v along glacier centerlines. Overall, glacier surface velocities across the study region were generally slow, with nearly 90% of glaciers flowing at rates below 50 m a^{-1}. Faster glacier flow was primarily concentrated in the maritime zone, particularly in the Hengduan and Nyainqentanglha Mountains. In other regions, glacier surface velocities exhibited more heterogeneous patterns.

When compared to the velocity thresholds defined in the Shi–Xie classification, most glacierized regions (85% of glaciers) experienced significant slowdowns, falling below the thresholds for their respective glacier types during the period 1981–2000. Only about 15% of glaciers remained within their thresholds, and these were scattered across all three glacier types. Notably, no glaciers exhibited speedup during this period.

4.2.2. Distribution over the Period 2001–2019

Figure 5 shows the spatial distributions of ELAs and the classification criteria for the period 2001–2019. As the ELAs rise, the 2 m air temperature at the ELAs decreases due to

the adiabatic lapse rate, which partially offsets the effects of climate warming. Consequently, the criteria T_a, T_s, and T_{20} for 2001–2019 (Figure 5b,c,e) show similar positive or negative variations relative to the classification thresholds to those for 1982–2000 (Figure 4b,c,e). For the annual precipitation averaged over 2001–2019, it shows significant increase partially due to the ELA rise (Figures 4d and 5d). However, the spatial pattern of P_a also exhibits comparable increases or decreases relative to the classification thresholds, consistent with those observed for the period 1982–2000. When compared to the thresholds of surface velocity (v), the spatial pattern of v during the period 2001–2019 was similar to that observed in 1982–2000 (Figures 4f and 5f). Most glaciers experienced a slowdown, with their velocities falling below the respective thresholds. Only seven glaciers maintained stable velocities within their thresholds, while two subcontinental glaciers in the Kunlun Mountains exhibited acceleration, surpassing their thresholds.

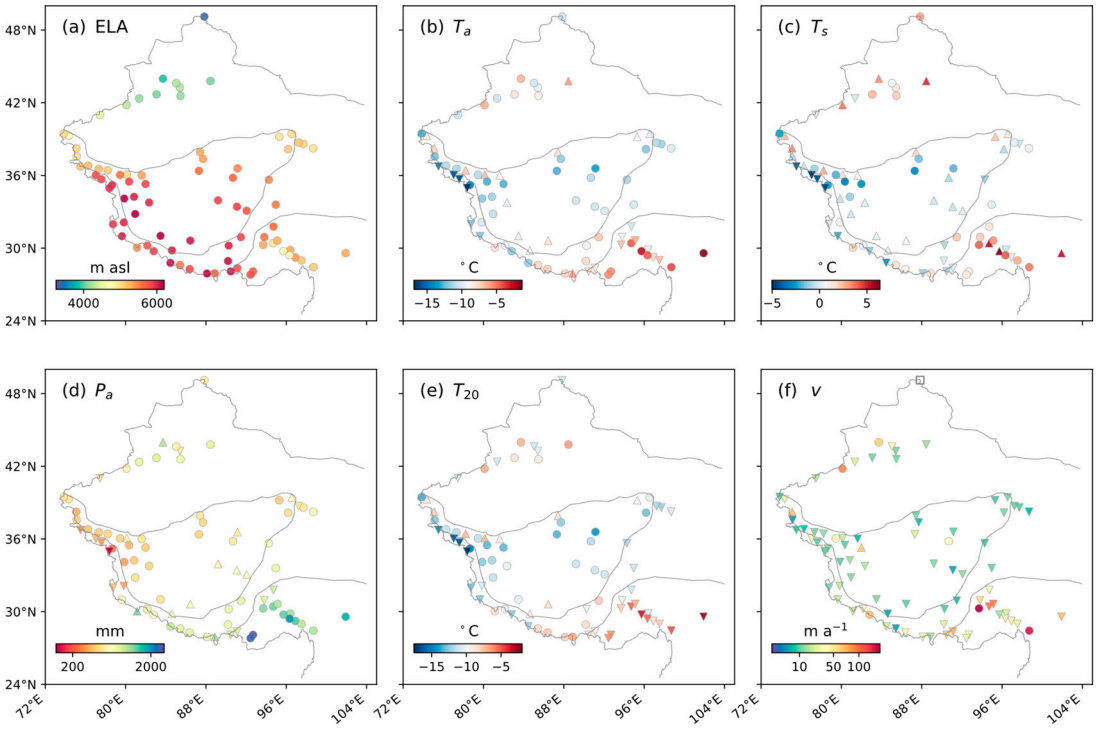

Figure 5. Same as Figure 4, but for the period 2001–2019. (**a**–**f**) The colorbar scale for each panel matches that of the corresponding panel in Figure 4.

4.2.3. Changes Between the Two Periods

We further analyzed the differences in the ELA and the five classification criteria between the periods 2001–2019 and 1982–2000 (Figure 6). ELAs increased for all glaciers during 2001–2019, ranging from 21 to 205 m compared with the period 1982–2000 (Figure 6a). The largest ELA rises (>90 m) occurred in the Qilian Mountains, Karakoram, and western Himalayas, while smaller increases (<50 m) were observed in the western Kunlun Mountains and the southern and eastern TP. This spatial heterogeneity in ELA rise was particularly pronounced in the Karakoram region, where the large ELA increase was also associated with corresponding decreases in air temperature at the ELA.

The difference map of the annual mean 2 m air temperature at the ELA (ΔT_a) (Figure 6b) reveals that 46.25% of glaciers (37 out of 80) experienced cooling ($\Delta T_a < -0.1$ °C) during 2001–2019 compared to 1982–2000. These glaciers, spanning various mountain ranges and glacier types, were primarily distributed in the Himalayas, inner TP, and Qilian Mountains, with 84% classified as continental glaciers. On average, their ELAs rose by 92.4 m relative to the earlier period. In contrast, 12.5% of glaciers (10 out of 80) exhibited

warming (ΔT_a > +0.1 °C), mostly located in the western Kunlun Mountains and Tien Shan, with a mean ELA increase of 58.5 m. More than 40% of glaciers showed relatively stable T_a values ($|\Delta T_a| < 0.1$ °C), primarily in the southeastern glacierized regions, including Nyainqentanglha, Hengduan Mountains, and the eastern Himalayas, as well as the Pamir–Karakoram–Kunlun Mountains regions, with a mean ELA rise of 70.7 m.

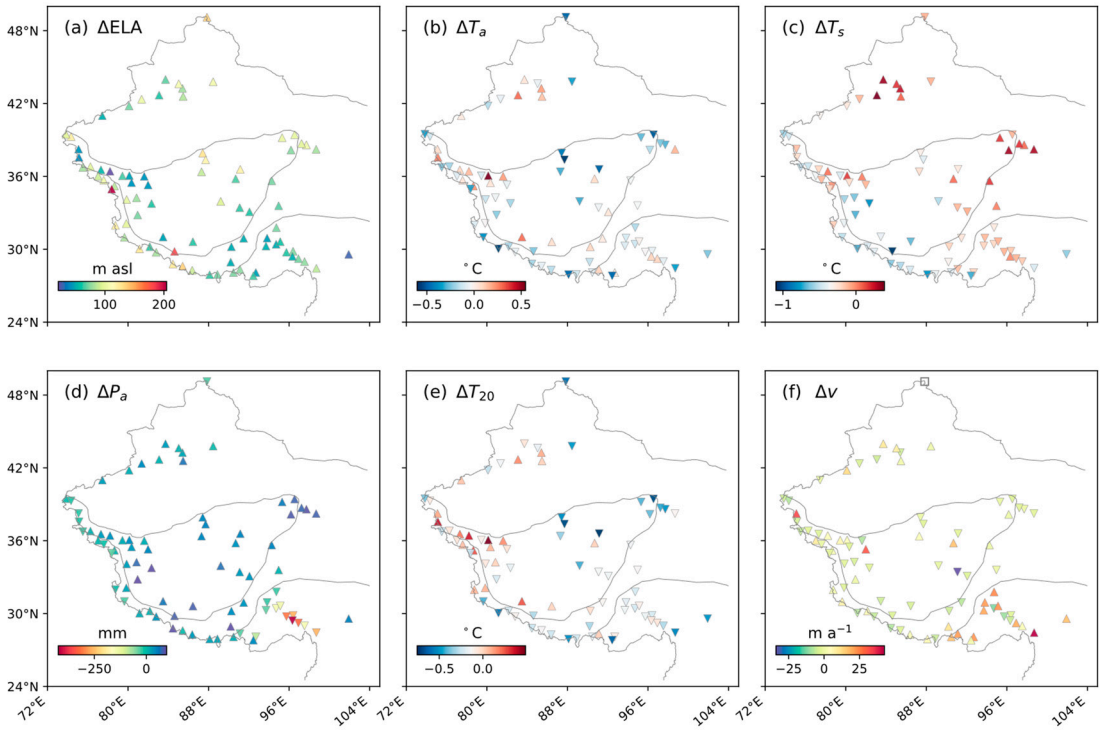

Figure 6. Difference maps of ELA and classification criteria between the periods 2001–2019 and 1982–2000. (**a**) ΔELA, (**b**) ΔT_a, (**c**) ΔT_s, (**d**) ΔP_a, (**e**) ΔT_{20}, (**f**) Δv. Upper (lower) triangles indicate that the differences are positive (negative). The square in panel (**f**) indicates no velocity data for this glacier. T_a, (**c**) T_s, (**d**) P_a, (**e**) T_{20}, (**f**) v.

For summer mean temperature at the ELA (ΔT_s), 67.5% of glaciers experienced cooling ($\Delta T_s < -0.1$ °C), with an average change of −0.40 °C, while 12.5% showed warming (ΔT_s > +0.1 °C), averaging +0.25 °C (Figure 6c). In contrast, 20% of glaciers exhibited relatively stable summer temperatures ($|\Delta T_s| < 0.1$ °C). These glaciers were sparsely distributed, with a mean ELA rise of 71.7 m. Glaciers in the Himalayas, Karakoram, Pamir, most of the inner TP, and many maritime glaciers showed a decrease in T_s, with a mean ELA rise of 81.6 m. In contrast, glaciers in the Tien Shan, Qilian Mountains, and eastern Kunlun Mountains experienced an increase in T_s, with an average ELA rise of 78.3 m.

Precipitation changes at the ELA (ΔP_a) displayed notable divergence (Figure 6d). Approximately 27.5% of glaciers experienced a decrease in precipitation ($\Delta P_a < 0$ mm), with most of these glaciers being maritime types and some located from the Pamir to the western Himalayas. A pronounced precipitation decrease occurred in the Hengduan Mountains, with a mean ΔP_a of −288.7 mm. In contrast, 72.5% of glaciers exhibited an increase in precipitation at the ELA ($\Delta P_a > 0$ mm), mostly under 100 mm. Despite these differing precipitation trends, the mean ELA rise was similar for both groups: 79.1 m for glaciers with increased precipitation and 79.4 m for those with decreased precipitation.

The temporal variation in the 20 m ice temperature at the ELA between the two periods (ΔT_{20}) ranged from −0.75 °C to 0.49 °C (Figure 6e). The spatial patterns of ΔT_{20} and ΔT_a were largely similar, except for a small subset of 11 glaciers (Figure 6b,e). These glaciers exhibited an increasing trend in near-surface ice temperature ($\Delta T_{20} > 0$) compared to the

decreasing trend in annual mean 2 m air temperature ($\Delta T_a < 0$). Such glaciers were sparsely distributed across Chinese glacierized regions, with a relatively higher concentration among maritime glaciers.

Figure 6f shows the glacier velocity changes between the two periods (Δv). Approximately 44.3% of glaciers accelerated ($\Delta v > 0$), while 55.7% decreased ($\Delta v < 0$). Using a ± 1.6 m a^{-1} uncertainty threshold for satellite-derived surface velocities [8], glaciers were classified as speeding up ($\Delta v > +1.6$ m a^{-1}), slowing down ($\Delta v < +1.6$ m a^{-1}), or stable ($|\Delta v| \leq 1.6$ m a^{-1}). We revealed that 46.8% of glaciers slowed, 35.5% sped up, and 17.7% remained stable during 2001–2019 compared to 1982–2000. Accelerated glaciers were primarily located in the Kunlun Mountains, characterized as extremely continental, and in southeastern glacierized regions, including the Hengduan Mountains, Nyainqentanglha, and eastern Himalayas, which were predominantly maritime. Decelerated glaciers were broadly distributed across the study area, whereas stable glaciers were scattered without a clear geographical concentration.

4.3. Threshold-Based Transformation in Glacier Types

In this section, we assess glacier type transformation based on deviations from the classification thresholds. Here, transformation refers to substantial changes in a glacier's climate, thermal, and dynamic characteristics without necessarily implying a complete shift from one glacier type to another. By quantifying the number of criteria exceeding their respective thresholds, we evaluate the intensity of transformation. Glaciers with three or more criteria deviating from their type-specific thresholds are considered to have undergone significant transformation.

Figure 7 illustrates the spatial distribution of glaciers deviating from classification thresholds during the periods 1982–2000 and 2001–2019. The overall pattern remained relatively consistent across both periods. Glaciers with the highest number of deviations were primarily concentrated in the Karakoram, western Kunlun Mountains, Qilian Mountains, and maritime glacierized regions. In contrast, only two glaciers in the first period and one in the second remained entirely within the classification thresholds, all of which belong to the extremely continental type. Notably, glaciers with all five classification criteria exceeding the thresholds were clustered in the Karakoram and western Kunlun Mountains, underscoring these regions as key transition zones. Glaciers in the Tien Shan and inner TP showed relatively fewer deviations from the thresholds, while those at the boundaries between glacier types exhibited a marked increase in classification deviations.

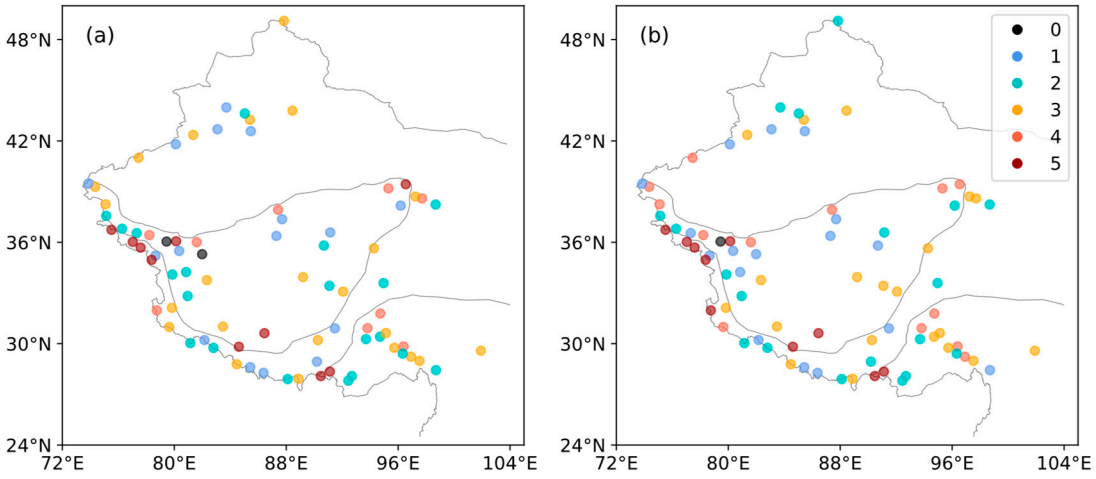

Figure 7. Number of criteria deviating from the classification thresholds across two time periods. (**a**) 1982–2000. (**b**) 2001–2019.

Among extremely continental glaciers, those along the Kunlun–Qilian transect and in the Gangdise and Tanggula Mountains near the subcontinental boundary exhibited more than three criteria exceeding the classification threshold. The former group primarily deviated in T_a, T_s, P_a, and T_{20}, while the latter mainly deviated in T_a and T_s. These glaciers generally had surface velocities below the extremely continental threshold. Subcontinental glaciers in the Karakoram displayed all five criteria below the threshold, closely resembling extremely continental glaciers. In contrast, glaciers in the Tien Shan and Altai Mountains typically deviated in two criteria, i.e., T_{20} and v were lower, while T_s was higher than the threshold, reflecting distinct differences in thermal and dynamic characteristics. Maritime glaciers near the subcontinental boundary in the eastern Himalayas and southern and eastern TP predominantly showed P_a, T_{20}, and v below thresholds, indicating similarities with subcontinental glaciers. Similarly, glaciers in the Hengduan Mountains tend to have three criteria (i.e., T_a, T_{20}, and v) falling below the threshold, suggesting a shift toward more continental characteristics.

5. Discussion

5.1. Drivers of Glacier Criteria Changes

Changes in glacier classification criteria across China from 1982 to 2019 reveal emerging tendencies toward glacier type transformations. Glacier classification is governed by climatic, thermal, and dynamic factors, and their temporal changes should be interpreted in the context of changes in large-scale circulation systems, regional climate regimes, glacier morphology like topography, and glacier dynamic processes.

ELA plays a pivotal role in glacier classification, as four of the five criteria in the Shi–Xie scheme are defined at the equilibrium line. Under sustained glacier mass loss, the ELA across China's glacierized regions has exhibited a rising trend [6,42], with a marked acceleration after 2000. This rise is primarily driven by enhanced ablation due to rising air temperatures and reduced solid precipitation [43,44]. However, the rate and spatial pattern of ELA changes vary across glacier types. For continental glaciers, ELA rise is mainly linked to decreased precipitation resulting from weakened westerlies and monsoonal activity [45]. For maritime glaciers, the mass loss and resulting ELA rise after 2000 were mainly caused by the decreased solid precipitation ratio and precipitation amount during the monsoon season [46]. The magnitude of ELA rise is a direct indicator of glacier sensitivity to climate forcing [47,48]. Since four criteria in the Shi–Xie scheme are defined at the ELA, any shift in the ELA due to climatic forcing directly propagates through the classification system.

ELA variations regulate the elevation at which climatological and thermal classification criteria are assessed, thereby interacting with the atmospheric lapse rate and orographic effects. When the ELA rises substantially, the cooling induced by the lapse rate can offset or even exceed the background atmospheric warming, resulting in a lower mean annual and summer temperature at the ELA. This elevation-driven cooling helps explain why some glaciers, despite experiencing regional warming, exhibit decreasing temperatures at their ELA. Conversely, when the ELA rises only slightly, the effect of background warming dominates, leading to temperature increases at the ELA. In addition, the ELA may rise into elevations subject to stronger orographic uplift, which enhances condensation and local precipitation. This mechanism partly accounts for the slight increases in ELA precipitation observed in transitional glacier regions. Thus, ELA variations not only reflect climatic changes, but also introduce elevation-related effects on temperature and precipitation metrics. Precipitation patterns across the TP reflect a warm–wet shift, shaped by the interplay of monsoonal systems, westerlies, and local circulation [49,50]. Across the eastern semi-arid to semi-humid regions, increased precipitation enhanced glacier accumulation. Conversely, in maritime glacier regions, weakened Indian monsoons and reduced moisture transport

resulted in decreased precipitation and diminished mass input. However, in some areas such as the Kunlun and Qilian Mountains, local circulation adjustments slightly increased precipitation, promoting a transition toward subcontinental glacier characteristics [51]. Overall, maritime glaciers were characterized by relatively high temperatures and abundant precipitation, with their mass balance primarily sustained by snowfall. Extremely continental glaciers remained cold and arid, with low ablation rates and high thermal stability. Subcontinental glaciers, influenced by both westerlies and monsoons, displayed complex responses to climatic regime shifts, reflecting their transitional nature.

In this study, the 20 m ice temperature was simulated based on conductive heat transfer and was primarily controlled by the surface air temperature at the ELA [52,53]. An upward shift in the ELA effectively led to lower air temperatures at that altitude due to lapse rate effects, resulting in a corresponding decline in the modeled 20 m ice temperature. This cooling mechanism is particularly evident in regions with rapidly rising ELAs, such as the Himalayas, Hengduan Mountains, and southeastern TP. In contrast, regions like the Kunlun and Qilian Mountains, where ELA elevation remained relatively stable or warming was more pronounced, exhibited increasing ice temperatures. Overall, changes in 20 m ice temperature reflected the combined influence of ELA variability and regional climate trends. Notably, in maritime glacier regions characterized by frequent ELA fluctuations, significant cooling at the boundaries between glacier types suggested an ongoing thermal transition toward subcontinental glacier characteristics.

Glaciers of all types have generally experienced a reduction in surface velocity, with mean flow speeds falling below their respective dynamic thresholds. This slowdown was primarily caused by glacier thinning, which decreased ice thickness and thus lowered gravitational driving stress, weakening overall glacier dynamics [54–56]. Since 2000, glaciers across HMA have shown widespread and persistent deceleration. The decline in driving stress, largely controlled by changes in surface slope and ice thickness, was especially evident in areas with pronounced thinning [8]. Maritime glaciers, influenced by high precipitation and relatively warm ice temperatures under monsoonal climates, still maintain relatively high velocities in some regions. However, accelerated surface melting led to rapid thinning, which in turn caused significant reductions in flow speed. In contrast, continental glaciers located in cold and arid regions with low precipitation and ice temperatures exhibited low deformation capacity.

5.2. Limitations

While this study provides a comprehensive assessment of glacier transformations in China, several limitations should be acknowledged. These include uncertainties in ELA estimation due to limited observational data, potential biases in climate inputs from ERA5-Land reanalysis, and spatial and temporal gaps in glacier velocity datasets. Additionally, the small number of reference glaciers used for calibration and validation may affect the representativeness of our findings.

ELA is a key glaciological variable for deriving classification criteria in the Shi–Xie scheme. However, due to the limited availability of mass balance measurements, observed ELA data exist for only a few glaciers. To address this, we rely on SMB modeling using OGGM to estimate the ELA. Although the modeled ELAs were calibrated and validated using geodetic mass balance data, assessing their performance across different glacierized regions in China remains challenging due to regional variations in glacier–climate interactions.

The ERA5-Land reanalysis dataset is essential for calculating the climatological and thermal criteria in the Shi–Xie scheme. Despite its relatively high spatial resolution (9 km), temperature and precipitation estimates remain uncertain in glacierized regions with com-

plex topography and large elevation ranges. To introduce consistency between reanalysis dataset and glacier-scale topography, we used elevation-based downscaling methods to derive temperature and precipitation values at the ELA for each glacier. However, these methods introduce additional uncertainties. For temperature, we applied a constant lapse rate, yet in reality, lapse rates vary both spatially and temporally. For precipitation, we used regionally fitted precipitation gradients across sub-basins, but these may still fail to fully capture the fine-scale variability of orographic precipitation.

The ITS_LIVE glacier surface velocity dataset spans from 1985 to 2018, but its temporal coverage does not fully align with the climate dataset, which may introduce uncertainties in the analysis of glacier velocity–climate relationships. Additionally, ITS_LIVE has spatial data gaps, such as missing velocity data in the Altai Mountains, limiting its applicability in certain regions. Another source of uncertainty arises from the estimation of ice temperature at 20 m depth, which only accounts for conductive heat transfer and neglects more complex thermal processes, such as latent heat release from meltwater refreezing, which can influence the estimation of near-surface ice temperature.

This study relies on measurements from only six glaciers, which may limit the spatial representativeness of our assessment, particularly regarding the diversity of glacier types. Future research should integrate a broader range of in situ measurements, satellite observations, and model simulations (such as modeled ELA) to improve calibration and validation. Expanding the dataset will enhance the robustness of our assessment and provide a more comprehensive understanding of glacier transformations in China.

6. Conclusions

This study provides a comprehensive assessment of the spatial and temporal changes in the ELA and five glacier classification-related criteria for representative glaciers across China during 1982–2019. The results reveal regionally distinct glacier responses and evolving classification tendencies under climate change.

Overall, ELAs have risen across China, with the most significant increases observed in the Qilian Mountains, Karakoram, and western Himalayas. Despite ongoing warming, the altitude-induced cooling effect has led to declining air temperatures at the ELA for approximately 50% of the studied glaciers and summer temperature declines for 67.5%. Near-surface ice temperatures exhibit strong consistency with the observed changes in annual air temperature. Precipitation trends at the ELA show strong regional heterogeneity. While approximately 70% of glaciers experienced stable or slightly increasing annual precipitation, maritime glaciers, particularly those in southeastern regions, e.g., Hengduan Mountains, experienced significant decreases. In total, 90% of the studied glaciers flow at speeds below 50 $m \cdot a^{-1}$, indicating a widespread slowdown.

Glaciers near classification boundaries, particularly in the Karakoram, Qilian, and Hengduan Mountains, frequently exhibited multiple criteria deviations from their individual thresholds. Among extremely continental glaciers, the proportion exceeding classification thresholds rose by approximately 55% (from 31 to 48 glaciers), reflecting a shift toward subcontinental characteristics. In contrast, deviations in maritime glaciers declined by ~18% (from 49 to 40 glaciers), suggesting improved classification stability, though some retained subcontinental tendencies.

These findings highlight the critical role of regional climate variability in reshaping glacier characteristics and classification stability across China. By quantifying ELA shifts and threshold deviations, this study provides a baseline for predicting future glacier changes, with important implications for water resource management and climate adaptation strategies in vulnerable mountain regions.

Supplementary Materials: The following supporting information can be downloaded at https://www.mdpi.com/article/10.3390/rs17132289/s1. Table S1: Basic information of 80 sample glaciers; Table S2: Basic information of six glaciers used for calibration and validation; Table S3: Sources of partial indicator observation data and ELA data; Figure S1: Precipitation gradient distribution in level-7 basin [46,57–62].

Author Contributions: Conceptualization, Y.W. and T.L.; methodology, Y.W. and T.L.; writing—review and editing, Y.W., T.L., B.H., H.A., L.W., and W.S.; visualization, Y.W. and T.L. All authors have read and agreed to the published version of the manuscript.

Funding: This research was supported by the Young Doctoral Program Start-up Fund of Shandong Normal University, the Shandong Provincial Natural Science Foundation (Grant No. ZR2023QD078), and the National Natural Science Foundation of China (Grant No. 42271134).

Data Availability Statement: The RGI 6.0 glacier inventory is available at https://www.glims.org/RGI/randolph60.html (accessed on 1 December 2024). ERA5-Land reanalysis data can be accessed through the Copernicus Climate Data Store. The ITS_LIVE dataset can be accessed at https://nsidc.org/apps/itslive (accessed on 1 December 2024). The SRTM30_PLUS topography dataset is available at http://topex.ucsd.edu/WWW_html/srtm30_plus.html (accessed on 1 December 2024). OGGM-derived glacier centerline data are available from https://cluster.klima.uni-bremen.de/~oggm/assets/oggm_v1.4/centerlines_shapes (accessed on 1 December 2024). The sub-basin boundaries from HydroBASINS are available at https://www.hydrosheds.org/products/hydrobasins (accessed on 27 June 2025).

Acknowledgments: We would like to thank Jiawen Ren for his advice regarding the classification criteria.

Conflicts of Interest: The authors declare no conflicts of interest.

References

1. Guo, W.; Liu, S.; Xu, J.; Wu, L.; Shangguan, D.; Yao, X.; Wei, J.; Bao, W.; Yu, P.; Liu, Q.; et al. The second Chinese glacier inventory: Data, methods and results. *J. Glaciol.* **2015**, *61*, 357–372. [CrossRef]
2. Kang, E.; Liu, C.; Xie, Z.; Li, X.; Shen, Y. Assessment of glacier water resources based on the Glacier Inventory of China. *Ann. Glaciol.* **2009**, *50*, 104–110. [CrossRef]
3. Xiao, C.; Wang, S.; Qin, D. A preliminary study of cryosphere service function and value evaluation. *Adv. Clim. Change Res.* **2015**, *6*, 181–187. [CrossRef]
4. Yao, T.; Thompson, L.; Yang, W.; Yu, W.; Gao, Y.; Guo, X.; Yang, X.; Duan, K.; Zhao, H.; Xu, B.; et al. Different glacier status with atmospheric circulations in Tibetan Plateau and surroundings. *Nat. Clim. Change* **2012**, *2*, 663–667. [CrossRef]
5. Wang, N.; Yao, T.; Xu, B.; Chen, A.A.; Wang, W. Spatiotemporal pattern, trend, and influence of glacier change in Tibetan Plateau and surroundings under global warming. *Bull. Chin. Acad. Sci.* **2019**, *34*, 1220–1232. [CrossRef]
6. Shean, D.E.; Bhushan, S.; Montesano, P.; Rounce, D.R.; Arendt, A.; Osmanoglu, B. A Systematic, Regional Assessment of High Mountain Asia Glacier Mass Balance. *Front. Earth Sci.* **2020**, *7*, 363. [CrossRef]
7. Hugonnet, R.; McNabb, R.; Berthier, E.; Menounos, B.; Nuth, C.; Girod, L.; Farinotti, D.; Huss, M.; Dussaillant, I.; Brun, F.; et al. Accelerated global glacier mass loss in the early twenty-first century. *Nature* **2021**, *592*, 726–731. [CrossRef]
8. Dehecq, A.; Gourmelen, N.; Gardner, A.S.; Brun, F.; Goldberg, D.; Nienow, P.W.; Berthier, E.; Vincent, C.; Wagnon, P.; Trouvé, E. Twenty-first century glacier slowdown driven by mass loss in High Mountain Asia. *Nat. Geosci.* **2019**, *12*, 22–27. [CrossRef]
9. Deng, G.; Tang, Z.; Hu, G.; Wang, J.; Sang, G.; Li, J. Spatiotemporal Dynamics of Snowline Altitude and Their Responses to Climate Change in the Tienshan Mountains, Central Asia, during 2001–2019. *Sustainability* **2021**, *13*, 3992. [CrossRef]
10. Wang, J.; Tang, Z.; Deng, G.; Hu, G.; You, Y.; Zhao, Y. Landsat Satellites Observed Dynamics of Snowline Altitude at the End of the Melting Season, Himalayas, 1991–2022. *Remote Sens.* **2023**, *15*, 2534. [CrossRef]
11. Deng, G.; Tang, Z.; Dong, C.; Shao, D.; Wang, X. Development and Evaluation of a Cloud-Gap-Filled MODIS Normalized Difference Snow Index Product over High Mountain Asia. *Remote Sens.* **2024**, *16*, 192. [CrossRef]
12. Kääb, A.; Leinss, S.; Gilbert, A.; Bühler, Y.; Gascoin, S.; Evans, S.G.; Bartelt, P.; Berthier, E.; Brun, F.; Chao, W.-A.; et al. Massive collapse of two glaciers in western Tibet in 2016 after surge-like instability. *Nat. Geosci.* **2018**, *11*, 114–120. [CrossRef]
13. Yao, T.; Yu, W.; Wu, G.; Xu, B.; Yang, W.; Zhao, H.; Wang, W.; Li, S.; Wang, N.; Li, Z.; et al. Glacier anomalies and relevant disaster risks on the Tibetan Plateau and surroundings. *Sci. Bull.* **2019**, *64*, 2770–2782. [CrossRef]

14. An, B.; Wang, W.; Yang, W.; Wu, G.; Guo, Y.; Zhu, H.; Gao, Y.; Bai, L.; Zhang, F.; Zeng, C.; et al. Process, mechanisms, and early warning of glacier collapse-induced river blocking disasters in the Yarlung Tsangpo Grand Canyon, southeastern Tibetan Plateau. *Sci. Total Environ.* **2022**, *816*, 151652. [CrossRef]
15. Zheng, G.; Allen, S.K.; Bao, A.; Ballesteros-Cánovas, J.A.; Huss, M.; Zhang, G.; Li, J.; Yuan, Y.; Jiang, L.; Yu, T.; et al. Increasing risk of glacial lake outburst floods from future Third Pole deglaciation. *Nat. Clim. Change* **2021**, *11*, 411–417. [CrossRef]
16. Zhang, T.; Wang, W.; An, B.; Wei, L. Enhanced glacial lake activity threatens numerous communities and infrastructure in the Third Pole. *Nat. Commun.* **2023**, *14*, 8250. [CrossRef]
17. Zhang, G.; Carrivick, J.L.; Emmer, A.; Shugar, D.H.; Veh, G.; Wang, X.; Labedz, C.; Mergili, M.; Mölg, N.; Huss, M.; et al. Characteristics and changes of glacial lakes and outburst floods. *Nat. Rev. Earth Environ.* **2024**, *5*, 447–462. [CrossRef]
18. Su, B.; Xiao, C.; Chen, D.; Huang, Y.; Che, Y.; Zhao, H.; Zou, M.; Guo, R.; Wang, X.; Li, X.; et al. Glacier change in China over past decades: Spatiotemporal patterns and influencing factors. *Earth-Sci. Rev.* **2022**, *226*, 103926. [CrossRef]
19. Hagg, W. *Glaciology and Glacial Geomorphology*; Springer: Berlin/Heidelberg, Germany, 2022.
20. Shi, Y.; Xie, Z. Fundamental characteristics of modern glaciers in China. *Acta Geogr. Sin.* **1964**, *30*, 183–213. [CrossRef]
21. Lai, Z.; Huang, M. The fuzzy cluster analysis of glaciers in China. *Sci. Bull.* **1988**, *33*, 1250–1253. [CrossRef]
22. Shi, Y.; Liu, S. Estimation on the response of glaciers in China to the global warming in the 21st century. *Sci. Bull.* **2000**, *45*, 434–438. [CrossRef]
23. Qin, D.; Yao, T.; Ding, Y.; Ren, J. *Introduction to Cryospheric Science*; Springer: Singapore, 2021.
24. Wu, G.; Shen, Y. Glaciers tourism resources in China and their development. *J. Glaciol. Geocryol.* **2007**, *29*, 664–667. [CrossRef]
25. Li, Z.; Wang, F.; Li, H.; Xu, C.; Wang, P.; Zhou, P.; Yue, X. Science and Long-term Monitoring of Continental-type Glaciers in Arid Region in China. *Bull. Chin. Acad. Sci.* **2018**, *33*, 1381–1390. [CrossRef]
26. Ohno, H.; Ohata, T.; Higuchi, K. The influence of humidity on the ablation of continental-type glaciers. *Ann. Glaciol.* **1992**, *16*, 107–114. [CrossRef]
27. Fujita, K.; Ageta, Y.; Jianchen, P.; Tandong, Y. Mass balance of Xiao Dongkemadi glacier on the central Tibetan Plateau from 1989 to 1995. *Ann. Glaciol.* **2000**, *31*, 159–163. [CrossRef]
28. Bolch, T.; Yao, T.; Kang, S.; Buchroithner, M.F.; Scherer, D.; Maussion, F.; Huintjes, E.; Schneider, C. A glacier inventory for the western Nyainqentanglha Range and the Nam Co Basin, Tibet, and glacier changes 1976–2009. *Cryosphere* **2010**, *4*, 419–433. [CrossRef]
29. Shi, Y. *Concise Glacier Inventory of China*; Shanghai Popular Science Press: Shanghai, China, 2005.
30. Maussion, F.; Butenko, A.; Champollion, N.; Dusch, M.; Eis, J.; Fourteau, K.; Gregor, P.; Jarosch, A.H.; Landmann, J.; Oesterle, F.; et al. The Open Global Glacier Model (OGGM) v1.1. *Geosci. Model Dev.* **2019**, *12*, 909–931. [CrossRef]
31. Becker, J.J.; Sandwell, D.T.; Smith, W.H.F.; Braud, J.; Binder, B.; Depner, J.; Fabre, D.; Factor, J.; Ingalls, S.; Kim, S.H.; et al. Global Bathymetry and Elevation Data at 30 Arc Seconds Resolution: SRTM30_PLUS. *Mar. Geod.* **2009**, *32*, 355–371. [CrossRef]
32. Lange, S.; Menz, C.; Gleixner, S.; Cucchi, M.; Weedon, G.P.; Amici, A.; Bellouin, N.; Schmied, H.M.; Hersbach, H.; Buontempo, C.; et al. *WFDE5 Over Land Merged with ERA5 over the Ocean (W5E5 v2.0)*; ISIMIP Repository: Potsdam, Germany, 2021.
33. Cucchi, M.; Weedon, G.P.; Amici, A.; Bellouin, N.; Lange, S.; Müller Schmied, H.; Hersbach, H.; Buontempo, C. WFDE5: Bias-adjusted ERA5 reanalysis data for impact studies. *Earth Syst. Sci. Data* **2020**, *12*, 2097–2120. [CrossRef]
34. Huss, M.; Hock, R. A new model for global glacier change and sea-level rise. *Front. Earth Sci.* **2015**, *3*, 54. [CrossRef]
35. Lehner, B.; Grill, G. Global river hydrography and network routing: Baseline data and new approaches to study the world's large river systems. *Hydrol. Process.* **2013**, *27*, 2171–2186. [CrossRef]
36. Jiang, Y.; Yang, K.; Yang, H.; Lu, H.; Chen, Y.; Zhou, X.; Sun, J.; Yang, Y.; Wang, Y. Characterizing basin-scale precipitation gradients in the Third Pole region using a high-resolution atmospheric simulation-based dataset. *Hydrol. Earth Syst. Sci.* **2022**, *26*, 4587–4601. [CrossRef]
37. Jing, Z.; Zhou, Z.; Liu, L. Progress of the research on glacier velocities in China. *J. Glaciol. Geocryol.* **2010**, *32*, 749–754. [CrossRef]
38. Gardner, A.S.; Fahnestock, M.A.; Scambos, T.A. *ITS_LIVE Regional Glacier and Ice Sheet Surface Velocities: Version 1*; National Snow and Ice Data Center: Boulder, CO, USA, 2019. [CrossRef]
39. Friedl, P.; Seehaus, T.; Braun, M. Global time series and temporal mosaics of glacier surface velocities derived from Sentinel-1 data. *Earth Syst. Sci. Data* **2021**, *13*, 4653–4675. [CrossRef]
40. Millan, R.; Mouginot, J.; Rabatel, A.; Morlighem, M. Ice velocity and thickness of the world's glaciers. *Nat. Geosci.* **2022**, *15*, 124–129. [CrossRef]
41. Kienholz, C.; Rich, J.L.; Arendt, A.A.; Hock, R. A new method for deriving glacier centerlines applied to glaciers in Alaska and northwest Canada. *Cryosphere* **2014**, *8*, 503–519. [CrossRef]
42. Duan, K.; Yao, T.; Wang, N.; Shi, P.; Meng, Y. Changes in equilibrium-line altitude and implications for glacier evolution in the Asian high mountains in the 21st century. *Sci. China Earth Sci.* **2022**, *65*, 1308–1316. [CrossRef]
43. Yao, T.; Bolch, T.; Chen, D.; Gao, J.; Immerzeel, W.; Piao, S.; Su, F.; Thompson, L.; Wada, Y.; Wang, L.; et al. The imbalance of the Asian water tower. *Nat. Rev. Earth Environ.* **2022**, *3*, 618–632. [CrossRef]

44. Tang, Z.; Wang, X.; Deng, G.; Wang, X.; Jiang, Z.; Sang, G. Spatiotemporal variation of snowline altitude at the end of melting season across High Mountain Asia, using MODIS snow cover product. *Adv. Space Res.* **2020**, *66*, 2629–2645. [CrossRef]
45. Wang, R.; Liu, S.; Shangguan, D.; Radić, V.; Zhang, Y. Spatial heterogeneity in glacier mass-balance sensitivity across High Mountain Asia. *Water* **2019**, *11*, 776. [CrossRef]
46. Jouberton, A.; Shaw, T.E.; Miles, E.; McCarthy, M.; Fugger, S.; Ren, S.; Dehecq, A.; Yang, W.; Pellicciotti, F. Warming-induced monsoon precipitation phase change intensifies glacier mass loss in the southeastern Tibetan Plateau. *Proc. Natl. Acad. Sci. USA* **2022**, *119*, e2109796119. [CrossRef] [PubMed]
47. Arndt, A.; Schneider, C. Spatial pattern of glacier mass balance sensitivity to atmospheric forcing in High Mountain Asia. *J. Glaciol.* **2023**, *69*, 1616–1633. [CrossRef]
48. Rounce, D.R.; Hock, R.; Shean, D.E. Glacier mass change in High Mountain Asia through 2100 using the open-source python glacier evolution model (PyGEM). *Front. Earth Sci.* **2020**, *7*, 331. [CrossRef]
49. Huang, L.; Chen, J.; Yang, K.; Yang, Y.; Huang, W.; Zhang, X.; Chen, F. The northern boundary of the Asian summer monsoon and division of westerlies and monsoon regimes over the Tibetan Plateau in present-day. *Sci. China Earth Sci.* **2023**, *66*, 882–893. [CrossRef]
50. Yu, Y.; You, Q.; Zhang, Y.; Jin, Z.; Kang, S.; Zhai, P. Integrated warm-wet trends over the Tibetan Plateau in recent decades. *J. Hydrol.* **2024**, *639*, 131599. [CrossRef]
51. Johnson, E.; Rupper, S. An examination of physical processes that trigger the albedo-feedback on glacier surfaces and implications for regional glacier mass balance across high mountain Asia. *Front. Earth Sci.* **2020**, *8*, 129. [CrossRef]
52. Huang, M.; Shi, Y. Progress in the study on basic features of glaciers in China in the last thirty years. *J. Glaciol. Geocryol.* **1988**, *10*, 228–237. [CrossRef]
53. Paul, F.; Bolch, T.; Kääb, A.; Nagler, T.; Nuth, C.; Scharrer, K.; Shepherd, A.; Strozzi, T.; Ticconi, F.; Bhambri, R.; et al. The glaciers climate change initiative: Methods for creating glacier area, elevation change and velocity products. *Remote Sens. Environ.* **2015**, *162*, 408–426. [CrossRef]
54. Cuffey, K.M.; Paterson, W.S.B. *The Physics of Glaciers*; Academic Press: Cambridge, MA, USA, 2010.
55. Nanni, U.; Scherler, D.; Ayoub, F.; Millan, R.; Herman, F.; Avouac, J.-P. Climatic control on seasonal variations in mountain glacier surface velocity. *Cryosphere* **2023**, *17*, 1567–1583. [CrossRef]
56. Wallis, B.J.; Hogg, A.E.; Wessem, J.M.V.; Davison, B.J.; Broeke, M.R.V.D. Widespread seasonal speed-up of west Antarctic Peninsula glaciers from 2014 to 2021. *Nat. Geosci.* **2023**, *16*, 231–237. [CrossRef]
57. Wu, J.; Sun, W.; Huai, B.; Ding, M.; Wang, L.; Wang, Y.; Zhang, J.; Du, W.; Chen, J.; Qin, X. Mass Balance Reconstruction for Laohugou Glacier No. 12 from 1980 to 2020, Western Qilian, China. *Remote Sens.* **2022**, *14*, 5424. [CrossRef]
58. Loibl, D.; Richter, N.; Grünberg, I. Remote Sensing-Derived Time Series of Transient Snowline Altitudes for High Mountain Asia, 1986–2021. *arXiv* **2022**, arXiv:10.31223/X5WH2D.
59. Wanhua, Y.; Feiteng, W.; Zhongqin, L.; Hui, Z.H.; Chunhai, X.U.; Baojuan, H.U. Temporal and Spatial Distributions of the Equilibrium Line Altitudes of the Monitoring Glaciers in High Asia. *J. Glaciol. Geocryol.* **2016**, *38*, 1459–1469.
60. Wang, N.; He, J.; Pu, J.; Jiang, X.; Jing, Z. Variations in Equilibrium Line Altitude of the Qiyi Glacier, Qilian, over the Past 50 Years. *Chin. Sci. Bull.* **2010**, *55*, 3810–3817. [CrossRef]
61. Dong, Z.; Qin, D.; Ren, J.; Li, K.; Li, Z. Variations in the Equilibrium Line Altitude of Urumqi Glacier No. 1, Tianshan Mountains, over the Past 50 Years. *Chin. Sci. Bull.* **2012**, *57*, 4776–4783. [CrossRef]
62. Zhang, Y.; Hirabayashi, Y.; Liu, S. Catchment-Scale Reconstruction of Glacier Mass Balance Using Observations and Global Climate Data: Case Study of the Hailuogou Catchment, South-Eastern Tibetan Plateau. *J. Hydrol.* **2012**, *445*, 146–160. [CrossRef]